

Research

Inkjet-printed graphene oxide memory cells on paper for flexible electronics

Iulia Salaoru¹ · Myles Worsley² · George Fern^{2,3} · Shashi Paul^{1,2}

Received: 25 April 2024 / Accepted: 3 February 2025

Published online: 21 February 2025

© The Author(s) 2025 [OPEN](#)

Abstract

A number of two-dimensional (2D) materials have been explored for various applications, from electronic transistors to energy generation and storage. In this work, we explored the possibility of using reduced graphene oxide (rGO) in emerging two terminal memory devices using a printing technique. The fabricated memory devices were analysed using scanning electron microscopy, Raman spectroscopy, optical microscopy, and in-depth electrical measurements. We experimentally demonstrated that rGO memory devices fabricated via inkjet printing exhibit bipolar switching without the required electroforming step, with an on/off ratio of 3 orders of magnitude. The inkjet-printed approach allows for the layering of memory devices on each other, leading to an increase in information storage density.

Article highlights

- Reduced Graphene oxide memory devices were fabricated using an inkjet printing technology; potential to make 3- dimensional (3D) Memory.
- Silver and reduced graphene oxide printed patterns are uniform, continuous and display an excellent surface coverage.
- Reduced Graphene oxide based printed devices exhibit a bipolar switching with on/off ratio of 3 order of magnitude.

Keywords Inkjet printing · Silver ink · Reduced graphene oxide ink · Memory cells · Bi-stability · Retention time

1 Introduction

Memory devices are among the most widely used and essential electronics in today's world. Memory devices are important components of computers, health monitors, home appliances, defence and military technologies. A memory cell is an electronic device that is capable to display at least two distinct electrical states when an external stimulus is applied [1–3]. Two terminal and three terminal are the two common structures of memory devices. A large number of materials such as: transition metal oxides [4], chalcogenide [5], organic/small organic molecules [6, 7] and 2D materials were explored as active core of the memory cells [8–10]. Usually, researchers prefer to use a traditional/subtractive pathway to fabricate the organic/2D materials two terminal based memory cells by using thermal evaporation to deposit the

✉ Iulia Salaoru, spaul@dmu.ac.uk | ¹Emerging technologies research centre, De Montfort University, Leicester LE1 9BH, UK. ²Experimental techniques centre, Brunel University of London, Uxbridge UB8 3PH, UK. ³Department of chemical engineering, Brunel University of London, Uxbridge UB8 3PH, UK.



metal electrodes and spin coating to fabricate the active layer [10, 11]. From a manufacturing perspective, most of the traditional technologies require: heat generation in a deposition process, generation of chemical pollution, high vacuum, large amounts of electricity to run, wastage of a large volume of raw materials, mask required for patterning & fabrication of devices, and usually rigid substrates used and overall, a large carbon footprint is created. Recently, non-polluting and low energy consumption process are exploited in the fabrication of electronic devices with the main aim to reduce waste materials, energy and manufacturing costs. Printed electronics—Inkjet Printing (IJP) are emerging as an environmentally friendly and ecological pathway for the manufacturing of electronic devices. Reduction of wasted material, deposition of controlled amounts of material, digital and additive deposition, cost effectiveness, compatibility with a small to large area deposition are only few of the advantages of inkjet printing manufacturing [12, 13]. Due to these benefits, inkjet printing is currently investigated as sustainable alternative of traditional technologies for manufacturing of functional materials and electronic devices [8, 14, 15]. To date, inkjet printed graphene oxide-based memory cells were reported by Huber et al. [16]; however, these memory devices are based on spin on glass (SOG) as active core and use Poly(3,4-ethylenedioxythiophene)-poly(styrenesulfonate) (PEDOT:PSS) as electrode. Furthermore, Ag/GO/ITO memristor has been reported by Porro and Ricciardi [9]. In this work inkjet printing has been used to fabricate only the graphene oxide active core and the aluminum top contact has been deposited via traditional method (thermal evaporation). Recently, there have been few more reports on this subject [17–20]

In this work, inkjet printer technology was used to fabricate a cross bar architecture silver (Ag)/reduced (rGO)/silver (Ag) structure. Firstly, the viscosity, surface tension and pH of both inks (Ag and reduced GO) were investigated. Secondly, the Ag and rGO inks were inkjet printed and the surface coverage and uniformity of the printed pattern (multilayers) were assessed by optical microscopy and scanning electron microscopy (SEM). Furthermore, a full structure was fabricated using an additive layer manufacturing approach and the electrical characterising (i.e. current–voltage characteristic and memory retention time tests) were performed using a HP4140B-pico-ammeter. Raman Analysis was used to check the homogeneity of rGO in the films.

In the next section, we consider the methodology used to characterise the inks (Ag and rGO) and the Ag and rGO printed patterns, respectively. Furthermore, the fabrication and electrical characterisation of the Ag/rGO/Ag two terminal memory devices is covered. In Sect. 3 we discuss firstly, the rheological behaviour of Ag and rGO inks. Furthermore, the evaluation of the individual printed layers is provided. Yes, the protocol of printing memory cells as well as results of the electrical characterisation is included in this section. Finally, Sect. 4 provides the conclusions, including the limitations of this study and the future direction for this research.

2 Materials and methods

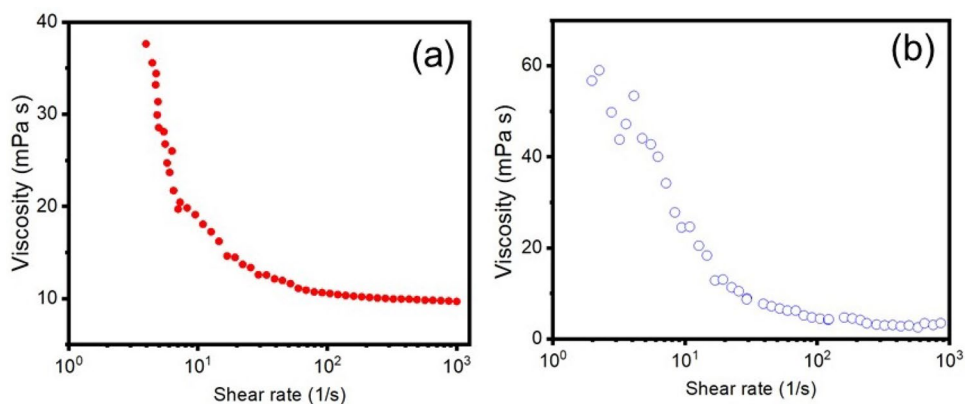
The first step was to assess the physical characteristics of both the Ag and reduced rGO inks. The rGO is stabilized with poly (sodium 4-styrenesulfonate), 10 mg/mL, dispersion in H₂O and was purchased from Sigma Aldrich. The nanoparticle silver (AgNPs) ink (Drycure Ag-j) is a mixture of (8–22) weight % Ag, (18–52) weight % water, (20–65) weight % glycerol and a small amount of alcohol. Furthermore, a non-organic (ceramic) coated paper has been used as substrate in this work. The paper substrate was purchased from Printed Electronics Ltd. and from here on it will be termed as “PEL paper”. Firstly, the surface tension of the inks was measured using a tensiometer (Torsion Balance) and was 35 mN/m for silver ink and 42 mN/m for rGraphene oxide, respectively. Furthermore, Jenway 3520-pH meter was used to test pH at 25 °C and was found 9 for Ag and 7.6 for rGo.

Furthermore, the rheological behaviour of both the inks was evaluated by a Bohlin, CVO 120HR rheometer.

Secondly, the wettability of both the Ag and rGO inks was assessed by measuring the contact angle (sessile drop method) between ink/substrate or ink/previously deposited layer (Attention Theta Optical Tensiometer, Biolin Scientific).

Printing rGO-based memory cells: Firstly, to prevent any sedimentation/agglomeration of Ag particles and rGO flakes both inks were sonicated for several hours before printing. Secondly, the EPSON T080X printer cartridge was then filled with Ag ink and a HP45 cartridge with rGO ink respectively. Ag multi-layer patterns were printed using an Epson Stylus P50 (a commercial desktop inkjet printer). The Epson Stylus P50 is a piezoelectric printer with the printhead having 90 nozzles, 65 µm nozzle diameter, 1.5 pL drop size and 360 dpi resolution. On the other hand, a thermal inkjet printer, ThallosJet Flatbed A3, was used to deposit rGO patterns. A HP45 printhead (Hewlett-Packard) with 300 nozzles, 28 µm nozzle diameter and 600 dpi resolution was used for printing of rGO patterns. A voltage pulse of 13 V with 2.5 µs pulse width was used to achieve a reliable printing process.

Fig. 1 Shear viscosity as a function of the shear rate of (a) Ag ink and (b) rGO ink



The electrical resistance and the sheet resistance of the 5-layer inkjet-printed silver films determined by traditional four-point probe Kelvin technique, are 6.63 $\Omega\cdot\text{cm}$ and 30.08 Ω/\square respectively.

In this work, two terminal memory devices with a cross bar architecture were fabricated via inkjet printing. For making the bottom electrode (BE), Ag (5 passes) conductive tracks were printed on the PEL paper. After printing, the curing of the deposited Ag conductive paths, took place at 120 °C/5 min. Then rGO active layer (10 passes) was printed onto Ag tracks/PEL paper and cured (80°C/20 min). Finally, brush-painting technique was used for the deposition on the the top electrode (TE) using silver ink. Brush-painting is a solution-based coating method and works by applying a small amount of ink on a narrow paintbrush [21]

Furthermore, an optical microscope (LAOPHOT-2) fitted with Nikon camera DS-Fi1 and high-resolution field emission gun scanning electron microscopy (FEG SEM) LEO Gemini 1525 were used to evaluate the quality of the printed patterns. The Renishaw Invia Micro Raman system fitted with a 514 nm laser was used to determine the uniformity of deposited rGO films.

Electrical characterisation of rGO printed memory device: The electrical behaviour of the fabricated Ag/rGO/Ag memory cells (current–voltage (I – V) characteristics and retention time test) was evaluated in a Faraday cage at room temperatures using a PC-driven HP4140B pico-ammeter.

3 Results and discussions

We proceed our study by printing and characterisation firstly the individual components of the two-terminal memory cells i.e. silver as electrode and reduced graphene oxide as active core. Secondly, a fully two terminal memory devices was fabricated and investigated. Previously, we use inkjet printing to fabricate PEDOT: PSS based memory devices [22] and silver was used as both the bottom and top electrode.

3.1 The rheological behaviour of Silver and rGO inks

We initially focus on understanding the rheological behaviour of both the Ag and rGO inks. A rotational (parallel plate) rheometer was used to measure the viscosities as a function of the shear rate. It is important to highlight that both the Ag and rGO tested inks display a shear thinning behaviour as the viscosities, at low-shear rates, decreased with increasing shear rate. As shown in Fig. 1(a) the viscosity of silver ink decreases from 37 mPa·s to 10 mPa·s as the shear rate increases from 1 to 50 s^{-1} and then a Newtonian behaviour is displayed at high shear rates. The same trend was displayed by rGO ink as can be seen in Fig. 1(b). As the shear rate approaching 10² s^{-1} , the shear viscosities are 10 mPa·s (Ag ink) and 4 mPa·s (rGo ink), respectively.

Fig. 2 **a** Optical microscopy images of inkjet printed Ag pattern **(a)** 3 passes **(b)** 5 passes **(c)** SEM images of 5 passes

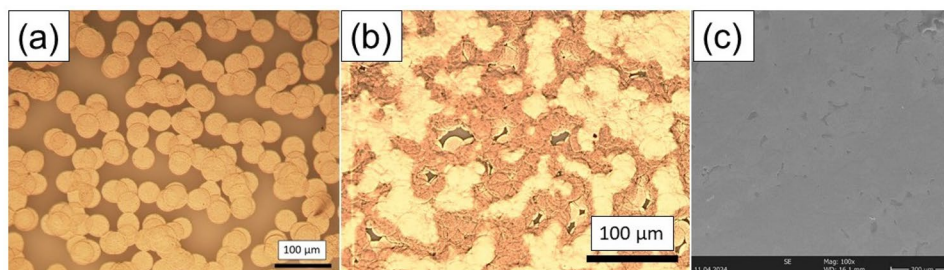
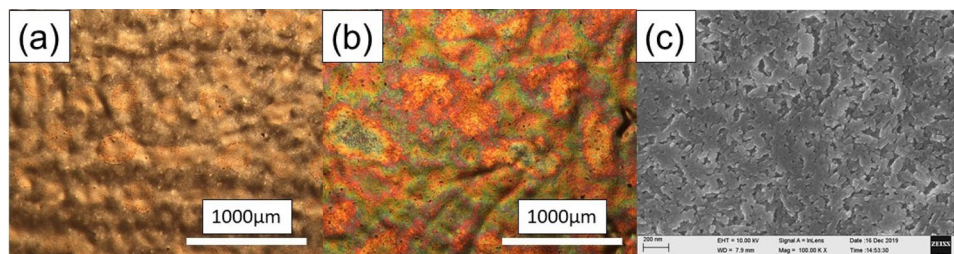


Fig. 3 Illustrates the Optical micrograph of inkjet printed rGO pattern **(a)** one pass **(b)** 5 passes **(c)** SEM images of 5 passes



3.2 Individual silver and rGO inkjet printed patterns:

Two terminal memory cells with cross-bar type architecture based on rGO sandwiched between two Ag electrodes (termed Ag/rGO/Ag) were fabricated using inkjet printing. We proceed our study by firstly printing and investigating the uniformity and coverage of the individual components i.e. silver and graphene oxide printed patterns. In our memory cells, the silver ink is used to fabricate both the top and bottom electrodes and the reduced graphene oxide is used as the active core of the memory elements. The reduces graphene oxide is selected as the active core for memory devices as it contains a number of defects, such as oxygen vacancies. The chemistry, i.e. the carbon: oxygen ratio of rGO, supports resistive switching without the need for electroforming.

The uniformity and the surface coverage of three and five printed passes (3 cm × 3 cm) printed squares were characterized by optical microscope and SEM. In Fig. 2, optical microscope images of silver printed layers are presented. As shown in the Fig. 2a, in a case of few passes (less than 4) the pattern achieved is not continuous and the coverage is poor. However, a better coverage was achieved when more than 5 passes of Ag ink were printed, and these results have not only positive impact on uniformity/coverage but as well on electrical properties of these patterns. As the Ag patterns are used as conductive tracks it's essential for the continuity of the patterns to be above the percolation threshold. The thickness of the silver patterns, achieved by 5 passes of Ag ink, was assessed via cross-sectional SEM image of the pattern and was found to be in the range of 1.1 and 1.8 μm and was previously reported [22]

Furthermore, the morphology of the rGO printed patterns were evaluated with the results presented in Fig. 3. It is evident that a great coverage was achieved when the rGO ink was printed. Both the optical micrograph and SEM images display rGO patterns with great coverage when more passes were printed. The SEM image, presented in Fig. 3(c), highlight a uniform and continuous pattern with interconnected flakes. It should be highlighted that the resistive losses are minimised in this type of pattern(s).

The Raman analysis of printed rGO is depicted in Fig. 4; peak D and G were observed separately on both the surface and edge of the printed film. This analysis is crucial in proving the uniformity of printed rGO films. We can also estimate the film thickness of 10 passes of rGO using Raman mapping from Fig. 4(c) and (d). It was found to be around 3 μm.

3.3 Printed fully two terminal memory devices

In two terminal memory devices, the active core is deposited between the bottom and top metal electrodes to form an array of memory cells. In this work, Ag ink is used to fabricate both the bottom and top electrodes, and rGO ink is used to create the active core. Prior to fabricating of the Ag/rGO/Ag memory cells the wettability of the: Ag ink

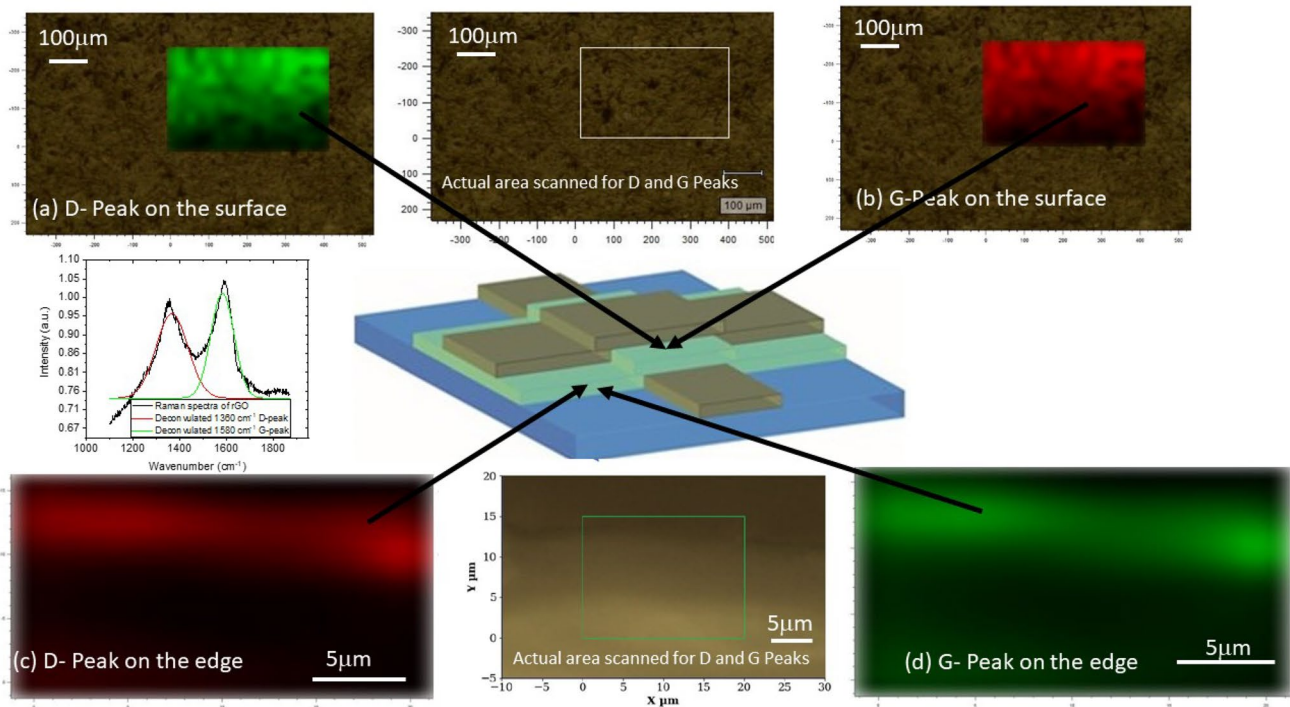
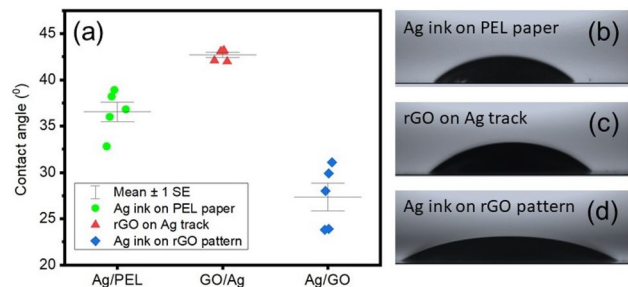


Fig. 4 Surface and edge profile of D (1360 cm^{-1}) and G (1580 cm^{-1}) Raman peaks of printed rGO. Both profiles demonstrate that the distribution of rGO in the memory sandwich structures is uniform

Fig. 5 a The results of contact angle measured via sessile drop analysis method; **(b)** photograph of Ag ink drop on PEL paper, **(c)** photograph of rGO drop on Ag track, **(d)** photograph of Ag drop on rGO pattern



on paper substrate, rGO on Ag tracks and Ag ink on rGO pattern was evaluated. Wettability evaluation is essential to ensure an excellent physical contact and hence an electrical continuity between preceding layers but as well to prevent electrical contact (short circuit) between bottom and top electrodes. Furthermore, the wettability is evaluated via contact angle measurement. As can be seen in Fig. 5 the Ag ink shows a good wettability on paper substrate and also on rGO pattern, with measured contact angles of mean 36° and 27° . Similarly, the rGO ink shows good wettability on the Ag track as it is observable in Fig. 5. The measured values of the contact angle ($0^\circ < \text{contact angle} < 90^\circ$) define a partial wetting that works perfectly with cross bar structure. Yet, a higher contact angle of Ag on paper (defining bottom electrode) when compare with the contact angle between the Ag and rGO (top electrode) ensure that the short circuit between top and bottom electrode do not occur.

Figure 6 illustrates the process steps involved in the inkjet printing of the cross-bar Ag/rGO/Ag memory cells. Firstly (step 1), the bottom silver track is inkjet printed using an Epson Stylus P50 printer. A ceramic coated paper was selected as substrate in this study. To ensure conductive patterns, 5 printed passes were performed and after that the printed tracks were cured at 120°C for 5 min. The second step in process of making two terminal memory devices represents the printing of rGO to form the active core. The rGO ink, 10 passes, was printed on the top of the Ag bottom electrodes. This step was completed with annealing at 80°C for 20 min. Finally, (step 3), the cross-bar structure is completed by deposition by brush-painting technique of Ag top contact onto the active core.

Fig. 6 Full process involved in the fabrication of Ag/rGO/Ag memory cells: middle images: schematic illustration of the fabrication flow-chart; left: photographs of the printed layers: Ag/PEL paper; rGO/Ag/PEL paper and a full structure Ag/rGO/Ag/PEL paper; Right: micrographs of the printed Ag/PEL paper, rGO/Ag/PEL paper and a full structure Ag/rGO/Ag/PEL paper

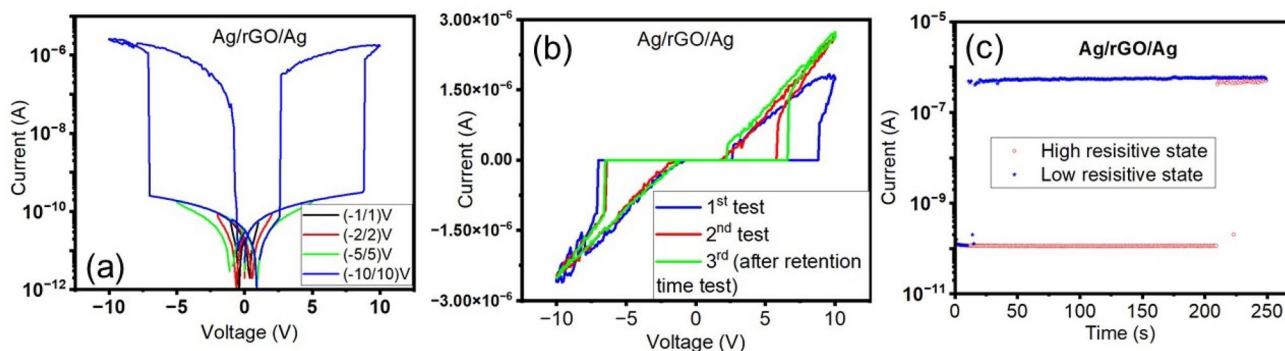
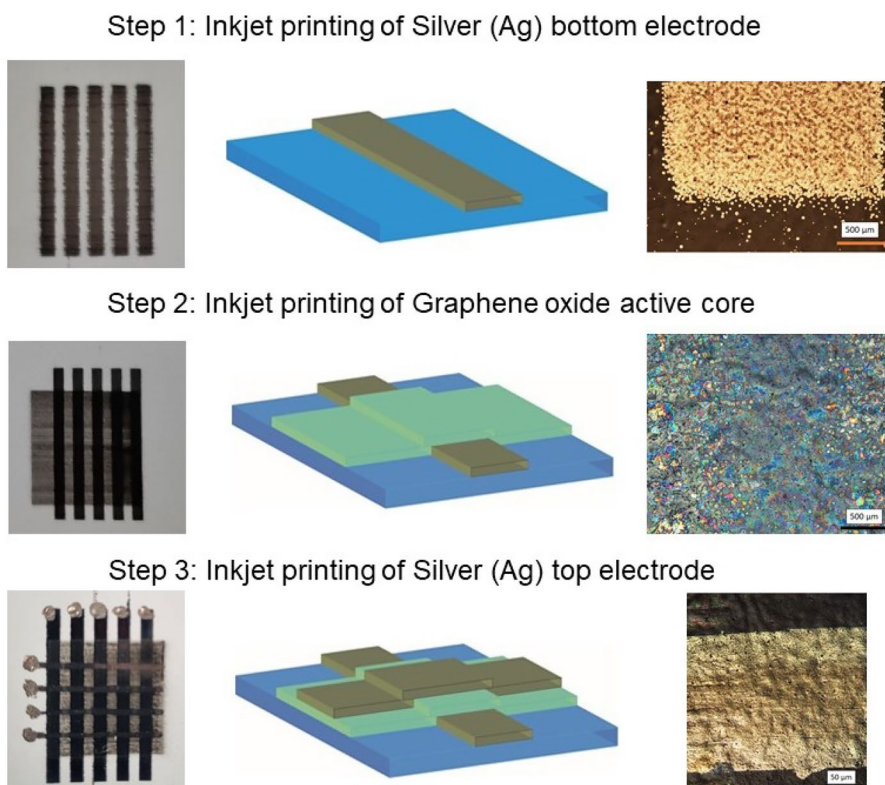


Fig. 7 Electrical behaviour of Ag/rGO/Ag memory cells: **a** & **b** Current–Voltage (*I*-*V*) behaviour of the memory elements **(c)** retention time of the memory devices

3.4 Electrical characterisation of rGO memory cells

The current–voltage characteristics of the printed memory cells were first evaluated via voltage sweeping with the results shown in Fig. 7. Electric field is the stimulus used in this work to activate/switch the rGO memory cells. The devices were biased via four consecutive switching cycles, commencing from 0 V that follow the sequence positive/negative in the applied potential. This testing protocol was used firstly to prevent the electrical breakdown of the memory cells and secondly to identify the suitable voltage to switch the devices from high resistive state to low resistive state. In Fig. 7(a), first cycle, represented by the black-colour curve, the voltage follows the sequence 0 V/+ 1 V back to 0 V and then – 1 V, and finally back to 0 V. Furthermore, the applied voltage is gradually increased with the 2nd cycle (in red), where the voltage

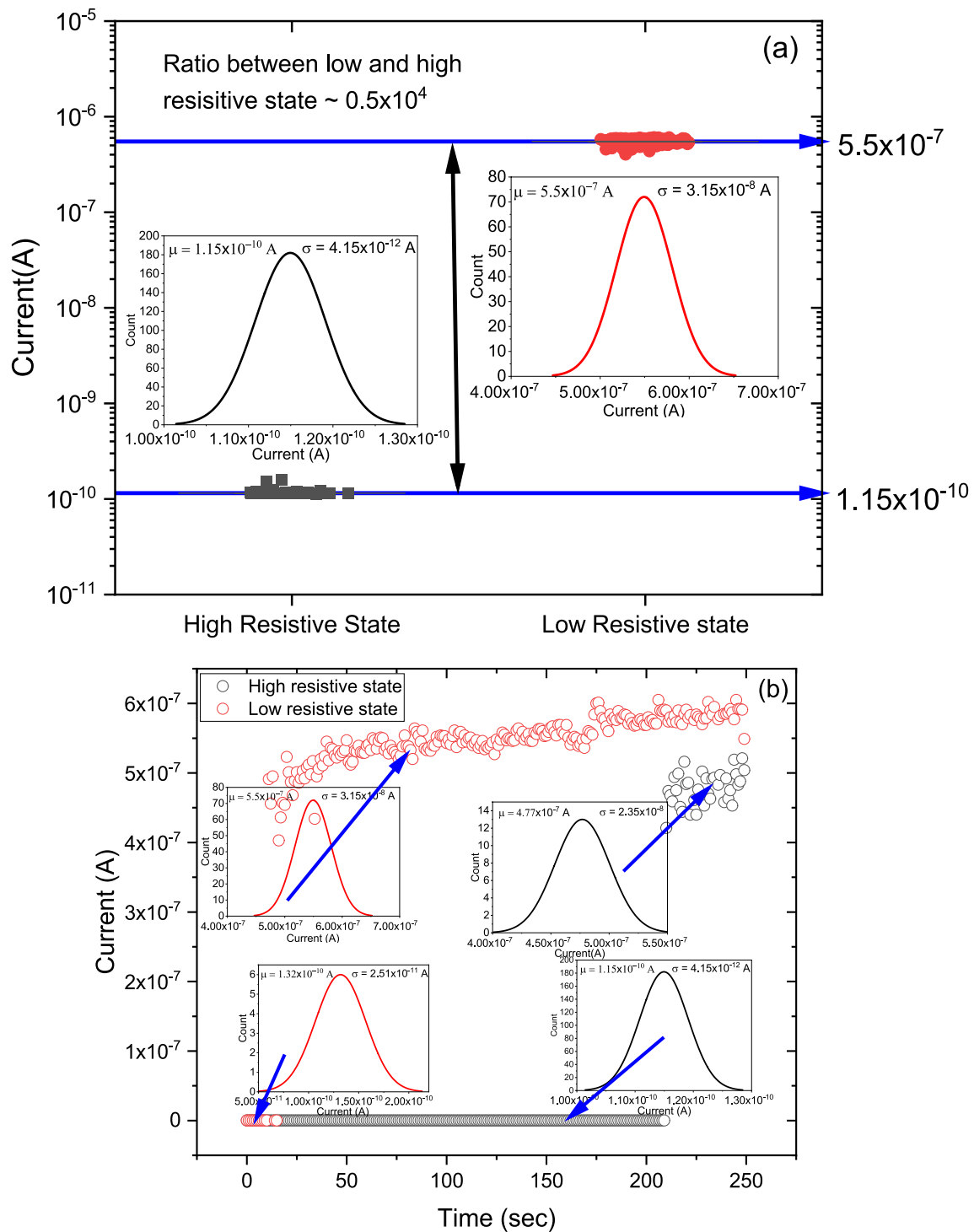


Fig. 8 **a** Interval plot of the retention behaviour of memory devices, along with the density distribution of high and low resistive states. **b** A retention plot that incorporates statistical analysis of clustered data for each state (where, μ is the mean and σ is the standard deviation)

was changed from 0 to 2 V and then from 2 V to - 2 V in an incremental step 0.1 V; 3rd (in green) where the maximum of +5/- 5 V is applied. The device is originally in a high resistive state (HRS) and the switching from HRS to low resistive state (LRS) takes place when a potential of + 10 V is applied. Reversing the voltage polarity to - 10 V reset the device to the high resistive state (HRS). This represents the 4th cycles, in blue, of the testing protocol and reversible resistive switching displayed by the cell follows a typical bipolar type of switching, as positive potential induces a change from

HRS to LRS, while the opposite happens for negative potentials. It is important to note, however, that the rGO based cells did not require any electroforming step. This behaviour was expected as the active core is rGO that means a number of defects, such as oxygen vacancies, exist and hence support the resistive switching without electroforming. This concept has been proved/demonstrated before in titanium dioxide memristor were by altering the stoichiometry of the active core can result in switching without electroforming[4]. Furthermore, the same device was tested via two consecutively cycles before and after the retention test, at (10 V/− 10 V) with the results included in Fig. 7(b). For the 2nd and 3rd cycles, less voltage is required to switch the device from HRS to LRS; and quite the same to reverse the device' state. The similar behaviour was observed in TiO₂ based memristor by Salaoru et al.[23].

From current–voltage (*I*-*V*) characteristics, *V*_{set}, *V*_{reset}, and *V*_{read} were identified. These values were further used during the memory retention time test, with the results presented in Fig. 7(c).

The device was programmed to a high resistive state ($I = 1.15 \times 10^{-10}$ A, as shown in Fig. 8(a)) by applying a pulse with an amplitude of 10 V, and this state was read at 6 V. Interestingly after 210 pulses, the device switches to a low resistive state (a cluster of such data points is shown in Fig. 8(a) with a mean value of current ($I = 4.77 \times 10^{-7}$ A). Furthermore, when reset pulse (− 10 V) is applied the device is now in the high resistive state and after 11 pulses moves to low resistive state. The density distribution of the first 11 pulses is also depicted in Fig. 8(b). The interval plot of HRS and LRS for a large portion of the pulses is shown in Fig. 8(a). Statistical analysis shows that the mean of each state has a 95% confidence interval. The retention time test demonstrates the coexistence of both bipolar and unipolar switching. This type of behaviour has been reported before in transition oxide metals-based memory devices [4, 9, 24, 25]. The statistical analysis presented in Fig. 8 for each state shows that the dispersion in the data is within the expected confidence limit, which provides encouragement for further exploration of GO into memory devices.

4 Conclusions

In conclusion, we have shown that additive layer manufacturing technology can be used to fabricate rGO memory devices. Both the electrodes (Ag) and the active core (rGO) were deposited via inkjet printing and firstly the properties of the inks and the printing parameters were investigated. Furthermore, the quality of the printed patterns in terms of uniformity and continuity was assessed. The electrical tests performed (current–voltage characteristics and retention time) of the Ag/rGO/Ag cross-bar structure clearly demonstrated that the printed cells display memory behaviour. Consequently, we have demonstrated that inkjet printing is a good alternative for the fabrication of memory devices and has the potential to replace traditional subtractive technologies. The limitation of our study is that the top silver contact is deposited by paint brush and the future direction is that the top contact to be deposited by inkjet printing and hence to use only inkjet printing to fabricate memory devices.

Acknowledgements The authors recognise and thank Dr Neil Chilton and Dr. Clare Conboy of Printed Electronics Ltd for their assistance in technical discussions. The authors also recognize and thank Dr. Ecaterina Ware of Imperial College London for assisting with the SEM image of the rGO printed pattern and Dr. Krishna Nama Manjunatha for assisting with electrical characterisation (Four-point probe Kelvin) of silver printed patterns.

Author contributions Iulia Salaoru conceived the experiments, printed the samples and performed the characterization of the inks, wettability and the electrical characterisation of the printed memory devices. Shashi Paul and Myles Worsley performed the Raman. The electrical behaviour of the memory devices was further examined by Shashi Paul. The first draft of the manuscript was written by Iulia Salaoru, and some parts of it were written by Shashi Paul. Changes and suggestions were made by George Fern to the manuscript. All authors commented on previous versions of the manuscript. All authors read and approved the final manuscript.

Funding We acknowledge funding from The Royal Society IES\R3\203157—International Exchanges 2020; The Royal Society SIF\R2\2320002—Royal Society Short Industry Fellowships and Higher Education Innovation Fund (HE00.11 & HE.0042.04) De Montfort University.

Data availability The corresponding author can provide data sets generated during the current study upon reasonable request.

Declarations

Competing interests The authors declare no competing interests.

Open Access This article is licensed under a Creative Commons Attribution-NonCommercial-NoDerivatives 4.0 International License, which permits any non-commercial use, sharing, distribution and reproduction in any medium or format, as long as you give appropriate credit to the original author(s) and the source, provide a link to the Creative Commons licence, and indicate if you modified the licensed material. You

do not have permission under this licence to share adapted material derived from this article or parts of it. The images or other third party material in this article are included in the article's Creative Commons licence, unless indicated otherwise in a credit line to the material. If material is not included in the article's Creative Commons licence and your intended use is not permitted by statutory regulation or exceeds the permitted use, you will need to obtain permission directly from the copyright holder. To view a copy of this licence, visit <http://creativecommons.org/licenses/by-nc-nd/4.0/>.

References

1. Paul F, Nama Manjunatha K, Paul S. Non-zero and open-loop current-voltage characteristics in electronic memory devices. *Adv Electron Mater*. 2023. <https://doi.org/10.1002/aelm.202300324>.
2. Paul F, Paul S. Electrical bistability by creating an internal electrical field and its application in emerging two-terminal electronic memory devices. *Royal Soc Chem Adv Memory Technol*. 2023. <https://doi.org/10.1039/BK9781839169946-00149>.
3. Paul S. Organic and macromolecular memory—nanocomposite bistable memory devices. *Adv Semicond Technol*. 2022. <https://doi.org/10.1002/9781119869610.ch8>.
4. Salaoru I, Khiat A, Li Q, Berdan R, Papavassiliou C, Prodromakis T. Origin of the off state variability in ReRAM cells. *J Phys D Appl Phys*. 2014. <https://doi.org/10.1088/0022-3727/47/14/145102>.
5. Sankir ND. Selective deposition of PEDOT/PSS on to flexible substrates and tailoring the electrical resistivity by post treatment. *Circuit World*. 2008;34(4):32–7. <https://doi.org/10.1108/03056120810918105>.
6. Paul F, Paul S. To be or not to be—review of electrical bistability mechanisms in polymer memory devices. *Small*. 2022. <https://doi.org/10.1002/sml.202106442>.
7. Lopera L, Rodriguez R, Yakout M, Elbestawi M, Emadi A. Current and potential applications of additive manufacturing for power electronics. *IEEE Open J Power Electr*. 2021;2:33–42. <https://doi.org/10.1109/OJPEL.2021.3052541>.
8. Rehman MM, Rehman HMMU, Gul JZ, Kim WY, Karimov KS, Ahmed N. Decade of 2D-materials-based RRAM devices: a review. *Sci Technol Adv Mater*. 2020;21(1):147–86. <https://doi.org/10.1080/14686996.2020.1730236>.
9. Porro S, Ricciardi C. Memristive behaviour in inkjet printed graphene oxide thin layers. *RSC Adv*. 2015;5(84):68565–70. <https://doi.org/10.1039/C5RA11058K>.
10. Pradhan SK, Xiao B, Mishra S, Killam A, Pradhan AK. Resistive switching behavior of reduced graphene oxide memory cells for low power nonvolatile device application. *Sci Rep*. 2016;6(1):26763. <https://doi.org/10.1038/srep26763>.
11. Yanagida T, et al. Scaling effect on unipolar and bipolar resistive switching of metal oxides. *Sci Rep*. 2013;3(1):1657. <https://doi.org/10.1038/srep01657>.
12. Khurana G, Kumar N, Chowalla M, Scott JF, Katiyar RS. Non-polar and complementary resistive switching characteristics in graphene oxide devices with gold nanoparticles: diverse approach for device fabrication. *Sci Rep*. 2019;9(1):15103. <https://doi.org/10.1038/s41598-019-51538-6>.
13. Kumar D, Aluguri R, Chand U, Tseng TY. Metal oxide resistive switching memory: Materials, properties and switching mechanisms. *Ceram Int*. 2017;43:S547–56. <https://doi.org/10.1016/j.ceramint.2017.05.289>.
14. Xie Y, Qi M, Xiu X, Yang J, Ren Y. Graphene oxide-based random access memory: from mechanism, optimization to application. *J Phys D Appl Phys*. 2023;56(3):033001. <https://doi.org/10.1088/1361-6463/aca2b5>.
15. Calvert P. Inkjet printing for materials and devices. *Chem Mater*. 2001;13(10):3299–305. <https://doi.org/10.1021/cm0101632>.
16. Huber B, Popp PB, Kaiser M, Ruediger A, Schindler C. Fully inkjet printed flexible resistive memory. *Appl Phys Lett*. 2017. <https://doi.org/10.1063/1.4978664>.
17. Li Y, et al. Aerosol jet printed WSe₂ crossbar architecture device on kapton with dual functionality as resistive memory and photosensor for flexible system integration. *IEEE Sens J*. 2020;20(9):4653–9. <https://doi.org/10.1109/JSEN.2020.2966547>.
18. Zhu K, et al. Inkjet-printed h-BN memristors for hardware security. *Nanoscale*. 2023;15(23):9985–92. <https://doi.org/10.1039/D3NR00030C>.
19. Peng Z, et al. Fully printed memristors made with MoS₂ and graphene water-based inks. *Mater Horiz*. 2024;11(5):1344–53. <https://doi.org/10.1039/D3MH01224G>.
20. Ding G, et al. Porous crystalline materials for memories and neuromorphic computing systems. *Chem Soc Rev*. 2023;52:7071–136. <https://doi.org/10.1039/D3CS00259D>.
21. Kim YJ, Yoon S, Cho Y-H, Kim G, Kim H-K. Paintable and writable electrodes using black conductive ink on traditional Korean paper (Hanji). *RSC Adv*. 2020;10(41):24631–41. <https://doi.org/10.1039/D0RA04412A>.
22. Salaoru I, Maswoud S, Paul S. Inkjet printing of functional electronic memory cells: a step forward to green electronics. *Micromachines*. 2019;10(6):417. <https://doi.org/10.3390/mi10060417>.
23. Salaoru I, Khiat A, Li Q, Berdan R, Prodromakis T. Pulse-induced resistive and capacitive switching in TiO₂ thin film devices. *Appl Phys Lett*. 2013. <https://doi.org/10.1063/1.4840316>.
24. Yuan L, Liu S, Chen W, Fan F, Liu G. Organic memory and memristors: from mechanisms, materials to devices. *Adv Electron Mater*. 2021. <https://doi.org/10.1002/aelm.202100432>.
25. Chen X, et al. Printed electronics based on 2D material inks: preparation, properties, and applications toward memristors. *Small Methods*. 2023. <https://doi.org/10.1002/smt.202201156>.

Publisher's Note Springer Nature remains neutral with regard to jurisdictional claims in published maps and institutional affiliations.